



The temporal event-based model: Learning event timelines in progressive diseases

Peter A. Wijeratne^{a,b}, Arman Eshaghi^c, William J. Scotton^d, Maitrei Kohli^a, Leon Aksman^e, Neil P. Oxtoby^a, Dorian Pustina^f, John H. Warner^f, Jane S. Paulsen^g, Rachael I. Scahill^h, Cristina Sampaioⁱ, Sarah J. Tabrizi^h, Daniel C. Alexander^a, for the Alzheimer's Disease Neuroimaging Initiative (ADNI), the Open Access Series of Imaging Studies (OASIS), the PREDICT-HD study, and the TRACK-HD study

^aUCL Centre for Medical Image Computing, Department of Computer Science, University College London, London, United Kingdom

^bDepartment of Informatics, University of Sussex, Brighton, United Kingdom

^cQueen Square Multiple Sclerosis Centre, Department of Neuroinflammation, University College London, London, United Kingdom

^dDementia Research Centre, Department of Neurodegenerative Disease, University College London, London, United Kingdom

^eKeck School of Medicine, University of Southern California, Los Angeles, California, United States

^fCHDI Management/CHDI Foundation, Princeton, New Jersey, United States

^gDepartments of Neurology and Psychiatry, Carver College of Medicine, University of Iowa, Iowa City, Iowa, United States

^hHuntington's Disease Centre, Department of Neurodegenerative Disease, University College London, Queen Square, London, United Kingdom

Corresponding Author: Peter A. Wijeratne (p.wijeratne@sussex.ac.uk)

ABSTRACT

Timelines of events, such as symptom appearance or a change in biomarker value, provide powerful signatures that characterise progressive diseases. Understanding and predicting the timing of events is important for clinical trials targeting individuals early in the disease course when putative treatments are likely to have the strongest effect. However, previous models of disease progression cannot estimate the time between events and provide only an ordering in which they change. Here, we introduce the temporal event-based model (TEBM), a new probabilistic model for inferring timelines of biomarker events from sparse and irregularly sampled datasets. We demonstrate the power of the TEBM in two neurodegenerative conditions: Alzheimer's disease (AD) and Huntington's disease (HD). In both diseases, the TEBM not only recapitulates current understanding of event orderings but also provides unique new ranges of timescales between consecutive events. We reproduce and validate these findings using external datasets in both diseases. We also demonstrate that the TEBM improves over current models; provides unique stratification capabilities; and enriches simulated clinical trials to achieve a power of 80% with less than half the cohort size compared with random selection. The application of the TEBM naturally extends to a wide range of progressive conditions.

Keywords: Disease progression model, Markov jump process, time series analysis, prognosis, neurodegeneration

1. INTRODUCTION

Progressive neurodegenerative conditions that lead to dementia affect 50 million people globally and this number is expected to double every 20 years, to approximately 66 million in 2030 and 115 million in 2050 (Prince et al., 2013). The global cost of dementia is currently estimated at over US\$1 trillion per year. Neurodegenerative

conditions such as Alzheimer's disease (AD) and Huntington's disease (HD) progress through various clinical and para-clinical changes, measurable through a range of biomarkers as the underlying disease pathology evolves. For example, current understanding of the pathological cascade in AD regards amyloid- β ($A\beta$) and tau pathology, captured by cerebrospinal fluid (CSF)

Received: 28 June 2023 Accepted: 15 July 2023 Available Online: 4 August 2023



The MIT Press

© 2023 Massachusetts Institute of Technology.
Published under a Creative Commons Attribution 4.0
International (CC BY 4.0) license.

Imaging Neuroscience, Volume 1, 2023
https://doi.org/10.1162/imag_a_00010

protein levels or positron emission tomography (PET) imaging, as early pathological changes, followed later by morphological changes in the brain, observable in structural magnetic resonance imaging (sMRI), then reduced performance on cognitive tests scores, and widespread personality changes and loss of cognitive function (Knopman et al., 2021). Although researchers have broad consensus on the ordering of these events, we have much less clarity on the absolute timing of transitions and how these timescales vary among patients.

Identifying the right time to recruit patients into clinical trials is a key challenge that has hindered the development of effective disease-modifying therapies. Almost all clinical trials in AD and HD have failed, at immeasurable human cost and financial cost in billions of dollars; the exceptions are a recent trial in AD that showed marginal treatment effects (<https://clinicaltrials.gov/ct2/show/NCT02477800>); and a recent trial in HD that showed initial promise but had to be stopped due to adverse side effects (<https://clinicaltrials.gov/ct2/show/NCT03761849>). A major barrier to the success of clinical trials is the inability to identify patients within the window of opportunity of a treatment to prevent, slow, or mitigate the pathological cascade. A quantitative timeline, based on measurable biomarkers, of how and when an individual's disease is likely to progress would enable clinical trialists to maximise the statistical power of detecting a treatment effect (i.e., the primary aim of clinical trials) by enriching trial cohorts for individuals likely to be at a disease stage amenable to treatment, and by more precisely quantifying a treatment effect against expected progression times.

Data-driven models of disease progression estimate long-term trajectories of biomarker changes using snapshots of biomarker measurements from collections of patients (Oxtoby & Alexander, 2017). Discrete disease progression models consist of a sequence of disease states, which capture the degree of biomarker abnormality at a discrete point along the disease trajectory (Fonteijn et al., 2012; Hadjichrysanthou et al., 2020; Liu et al., 2015; Sun et al., 2019; Williams et al., 2020; Young et al., 2018). The archetypal discrete disease progression model, the event-based model (EBM) of disease progression, describes disease progression as a sequence of biomarker events in which biomarkers transition from within some “normal” range to detectably abnormal (Fonteijn et al., 2012). The EBM and its extensions have revealed new insights in a range of diseases including AD (Firth et al., 2018; Fonteijn et al., 2012; Oxtoby et al., 2018; Venkatraghavan et al., 2019; Vogel et al., 2021; Young et al., 2014, 2018), HD (Wijeratne et al., 2018,

2021), multiple sclerosis (Eshaghi et al., 2018), Parkinson's disease (Oxtoby et al., 2021), prion disease (Pascuzzo et al., 2020), and amyotrophic lateral sclerosis (Gabel et al., 2020). They are also used practically to provide data-driven patient stratification (Eshaghi et al., 2021) and validate early biomarkers (Byrne et al., 2017, 2018). However, the EBM provides only an ordering of biomarker events; it contains no information on the time between events, which is a key limitation for stratifying patients suitable for clinical trials, that is, those likely to progress in the absence of treatment over the timescale of the trial. Moreover, the EBM does not naturally exploit longitudinal data, particularly when the number of time-points varies among individuals; the model treats each snapshot from one individual as independent, as if from a different individual, thereby ignoring strong within-individual correlations. This can introduce bias in the model, over-emphasising information from individuals with the most time-points.

Continuous disease progression models reconstruct continuous biomarker trajectories and are an alternative to discrete models (Bilgel & Jedynak, 2019; Donohue et al., 2014; Koval et al., 2021; Li et al., 2019; Lorenzi et al., 2019; O'Connor et al., 2020; Oxtoby et al., 2018; Schiratti et al., 2017; Staffaroni et al., 2022). While continuous disease progression models can theoretically encapsulate a more detailed picture of the disease timeline, discrete models remain popular in practice for two key reasons: i) simplicity—since they are defined by relatively few parameters and handle uncertainty and missing data naturally, they require relatively small data sets compared to continuous models, as few as 100 individuals (see e.g., Byrne et al., 2017; Oxtoby et al., 2018); and ii) interpretability—discrete models provide a discrete staging system that closely reflects the state-of-the-art staging systems used in clinical practice, e.g., the ATX(N) system in AD (Hampel et al., 2021) and the HD-ISS in HD (Tabrizi et al., 2022).

Here, we introduce the temporal event-based model (TEBM), a new probabilistic model that can uniquely learn the timing between biomarker events in progressive diseases and make probabilistic estimates of progression at the group and individual levels from sparse and irregularly sampled datasets (Fig. 1). The TEBM combines ideas from continuous-time hidden Markov modelling with event-based modelling, and it leverages the strengths of each methodology to provide a natural framework for learning timelines in progressive diseases. Moreover, unlike most disease progression models that only learn a disease stage per individual, the TEBM

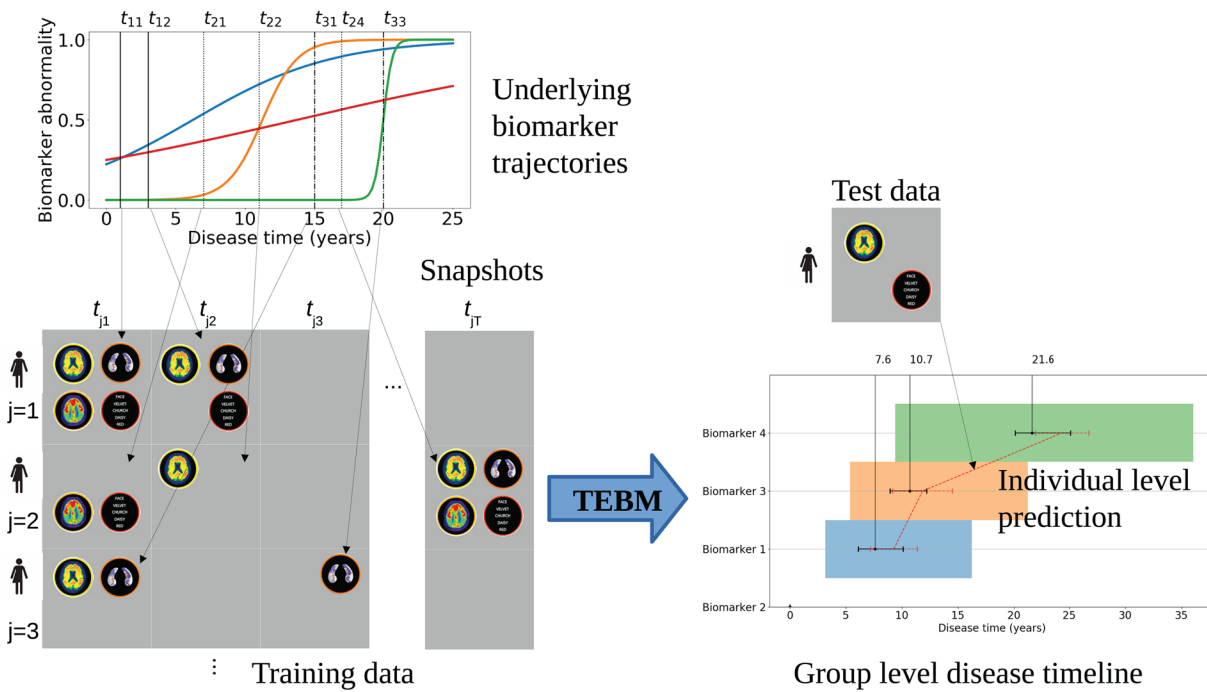


Fig. 1. The TEBM is designed to work with a typical semi-longitudinal dataset (left of figure). Patient measurements follow an underlying set of biomarker trajectories, which have some uncertainty in terms of timescale and ordering. A typical study will acquire data over a relatively short timescale compared to the full timeline of the disease. Thus, we acquire from each individual a number of biomarker snapshots at each of several time-points. Each time-point may miss some biomarker measurements; the number of time-points and their relative timings can vary among individuals. From such real-world data sets, the TEBM (right of figure) reconstructs an ordering of biomarkers showing abnormality together with mean and variance of times between consecutive events. This captures group-level behaviour and its variation. Given new data from a previously unseen individual, even a single time-point, the model provides an estimate of future transition times together with uncertainty for an individual.

allows us to learn both a disease stage, and a progression risk per individual, which can improve predictive utility. We use the TEBM to chart timelines of biomarker evolution in two neurodegenerative conditions, AD and HD, for which clinical trials of a variety of treatment strategies are highly active. We show the first discrete timelines of each disease that include transition times and ranges, providing new insight on the timescales and their variability over patient cohorts. With this in mind, we also benchmark the TEBM against the EBM and a state-of-the-art continuous-time disease progression model, the Gaussian Processes Progression Model (GPPM) (Lorenzi et al., 2019). Finally, we show how the TEBM can be used to enrich simulated clinical trials in AD with individuals who are most likely to progress rapidly and hence show a significant treatment effect during the trial. Crucially, we use the full capabilities of the TEBM to enrich preventative clinical trials, that is, trials on pre-clinical individuals, which are typically very difficult to power using standard methods.

2. RESULTS

First, we use simulated data to demonstrate the TEBM's ability to recover event timelines and its improvements over the EBM (see Supplementary Material Section 3). Next, we learn biomarker timelines and their temporal variability in AD and HD using the TEBM with data from the Alzheimer's Disease Neuroimaging Initiative (ADNI), and the TRACK-HD study in HD (Section 2.1). We replicate and validate the timelines in both diseases using external datasets: the Open Access Series of Imaging Studies (OASIS) in AD and the PREDICT-HD study in HD (Section 2.1).

As mentioned in the Introduction, the two key variables the trained TEBM assigns to each individual are i) disease stage and ii) progression risk; Methods section 4.11 defines both mathematically. We demonstrate the added power of this pair of predictive variables over the single stage variable of most current disease progression models. First, we demonstrate that they provide improved utility over two benchmark disease progression models

(Section 2.2). Next, we use them to stratify by genetic burden in HD (Section 2.3), and by clinical progression rate in AD (Section 2.4), using only baseline data. Finally, we demonstrate how the TEBM’s progression risk can be used to enrich simulated clinical trials in AD by dichotomising slow and fast progressing groups; and how both the TEBM’s progression risk and disease stage can be used to enable preventative clinical trials by dichotomising slow early-stage and fast early-stage groups (Section 2.5).

2.1. TEBM provides the first disease stage models with transition times in AD and HD

Figure 2a and b show unique timelines of events inferred by the TEBM in AD and HD, respectively. The timelines

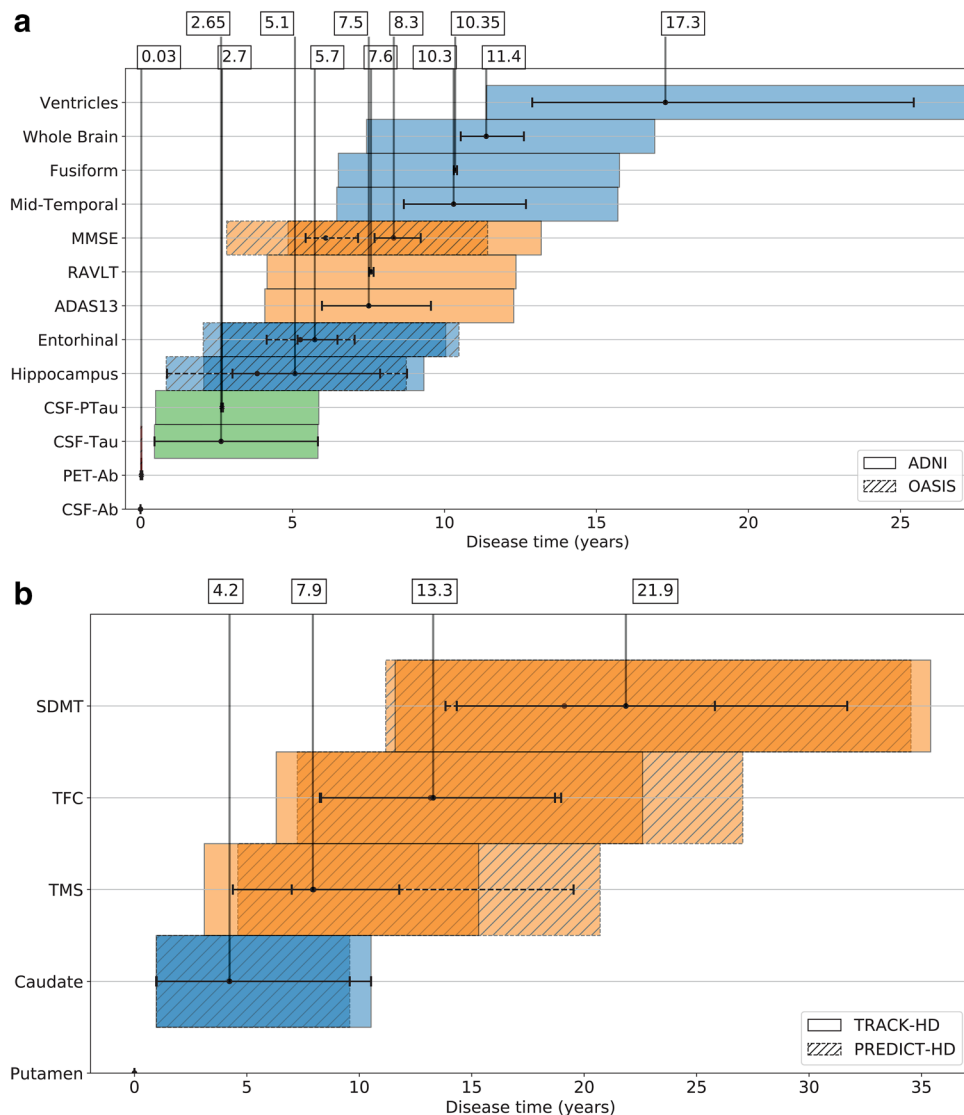


Fig. 2. Timelines of biomarker events in (a) AD, and (b) HD. The order of events on the vertical axis is obtained from the most likely sequence estimated by the TEBM and the mean time at which each event occurs relative to the first, shown by black dots on the horizontal axis, is calculated from the fitted transition generator matrix (\bar{S} and \bar{Q} in the Methods section 4.8). The uncertainty in the event duration, shown by black braces, represents 95% confidence intervals, and the uncertainty in the event timing relative to the first event is shown by colour bars, which are calculated as the cumulative uncertainty in the event duration propagated through the event sequence (described in the Methods section 4.12). Timelines are anchored at disease time equal to zero, which corresponds to the first event in the sequence. ADNI Dataset 1 and OASIS are used in (a), and TRACK-HD and PREDICT-HD in (b). The colour bars are coded according to the type of biomarker: green for CSF; blue for sMRI; and orange for clinical test score.

are anchored at disease time equal to zero, which corresponds to the first event in the sequence estimated by the TEBM. In AD, we use a selection of biofluid (CSF-based $A\beta$, CSF-based phosphorylated tau and total tau), imaging (PET-based $A\beta$, sMRI-based regional brain volumes), and cognitive markers (ADAS13, MMSE, RAVLT) from the ADNI dataset. In HD, we use a selection of imaging (sMRI-based regional brain volumes), motor (TMS), cognitive (SDMT), and functional (TFC) markers from the TRACK-HD dataset. For details on the biomarkers and datasets, see the Methods section. Supplementary Figure S1a and b show individual event-based trajectories predicted by the TEBM using only baseline data, from (a) the ADNI test dataset and OASIS dataset in AD, and (b) the PREDICT-HD dataset in HD. We estimate the disease time for MCIs in the OASIS dataset and PreHDs in the PREDICT-HD dataset at baseline, then compute the progression risk as a function of future time, which provides an estimated trajectory through the progression model. We also estimate uncertainty on that trajectory, as described in the Methods [section 4.12](#).

In AD, the TEBM finds a fine-grained chain of biomarker events occurring over a mean period of 17.3 years (95% confidence intervals (CIs): 11.4-27.1 years). In the ADNI dataset, we find that CSF- and PET-based $A\beta$ markers become abnormal approximately simultaneously within 0.03 years (95% CIs: 0-0.1 years); followed by CSF-based tau markers which also occur approximately simultaneously after 2.65 (95% CIs: 0.5-5.8 years) and 2.7 years (95% CIs: 0.5-5.9 years); followed by structural regional volume changes starting with the hippocampus at 5.1 years (95% CIs: 2.1-9.3 years) and the entorhinal at 5.7 years (95% CIs: 2.7-10 years); then first cognitive changes after 7.5 years (95% CIs: 4.1-12.3 years); followed by a chain of structural brain volume changes starting with the mid-temporal at 10.4 years (95% CIs: 6.5-15.7 years); and finally ventricular abnormality. We replicate the findings in a subset of biomarkers using an entirely independent dataset (OASIS), where we find the same ordering of changes and timings within 95% CIs. In HD, the TEBM finds a chain of biomarker events occurring over a mean period of 21.9 years (95% CIs: 11.6-35.4 years). In the TRACK-HD dataset, we find putamen volume abnormality occurs first; followed by caudate volume abnormality, which occurs after 4.2 years (95% CIs: 1-10.5 years); followed by motor abnormality after 7.9 years (95% CIs: 3.1-15.3 years); then functional abnormality after 13.3 years (95% CIs: 6.3-22.6 years); and finally cognitive abnormality. Again, we replicate our findings in an entirely independent HD dataset

(PREDICT-HD), where we find the same ordering of changes and timings within 95% CIs. In both AD and HD, we find that individuals progress along the predicted group-level timeline within 95% CIs, and that individuals within the same stage can progress at different rates.

[Figure 3](#) contrasts the information content of current state-of-the-art models estimated using the ADNI dataset with the output of the TEBM from [Figure 2](#). We find that the EBM recovers a similar overall ordering as the TEBM, but the TEBM also obtains both the mean and variability of transition times between consecutive events, plus an individual progression risk, which is not possible with the EBM. We find that the GPPM provides a broadly similar overall ordering of changes, though note that it is not primarily designed to estimate orderings but rather biomarker trajectories.

2.2. TEBM improves predictive utility over benchmark models in AD

To compare the practical utility of the TEBM to other models, we consider the task of identifying individuals who convert from a clinical diagnosis of MCI to AD at any time after their baseline measurement. First, we compare predictions of conversion using the TEBM stage only with predictions using stage from the EBM and GPPM. A simple approach uses the conversion rate of training individuals at each model stage to classify test individuals. With this approach, the area under the receiver operating characteristic curve (AU-ROC) and 95% confidence intervals from 5-fold cross-validation is $0.799 \pm (0.762, 0.835)$ for TEBM; $0.792 \pm (0.762, 0.822)$ for EBM; and $0.777 \pm (0.728, 0.825)$ for GPPM. However, the TEBM also provides an individual-level progression risk, which further informs the classification. Incorporating the additional progression risk into the classification task (see the Methods [section 4.11](#)), we obtain a substantially increased AUROC of $0.82 \pm (0.766, 0.873)$.

To further compare the TEBM to other models, [Supplementary Figure S2a](#) shows the observed age of AD conversion against the age of conversion predicted using the baseline metrics for each model. While the EBM is time-agnostic—and hence cannot predict age of conversion directly—the individual stage estimated using the EBM can be used with the observed age of conversion to train a model that predicts age of conversion (see the Methods [section 4.14](#)). Using this approach, the TEBM predicts conversion with an RMSE = 1.81 years; EBM with an RMSE = 1.9 years; and the GPPM with an RMSE = 2.14 years. However, we note that this approach depends on known age of conversion, as it uses models

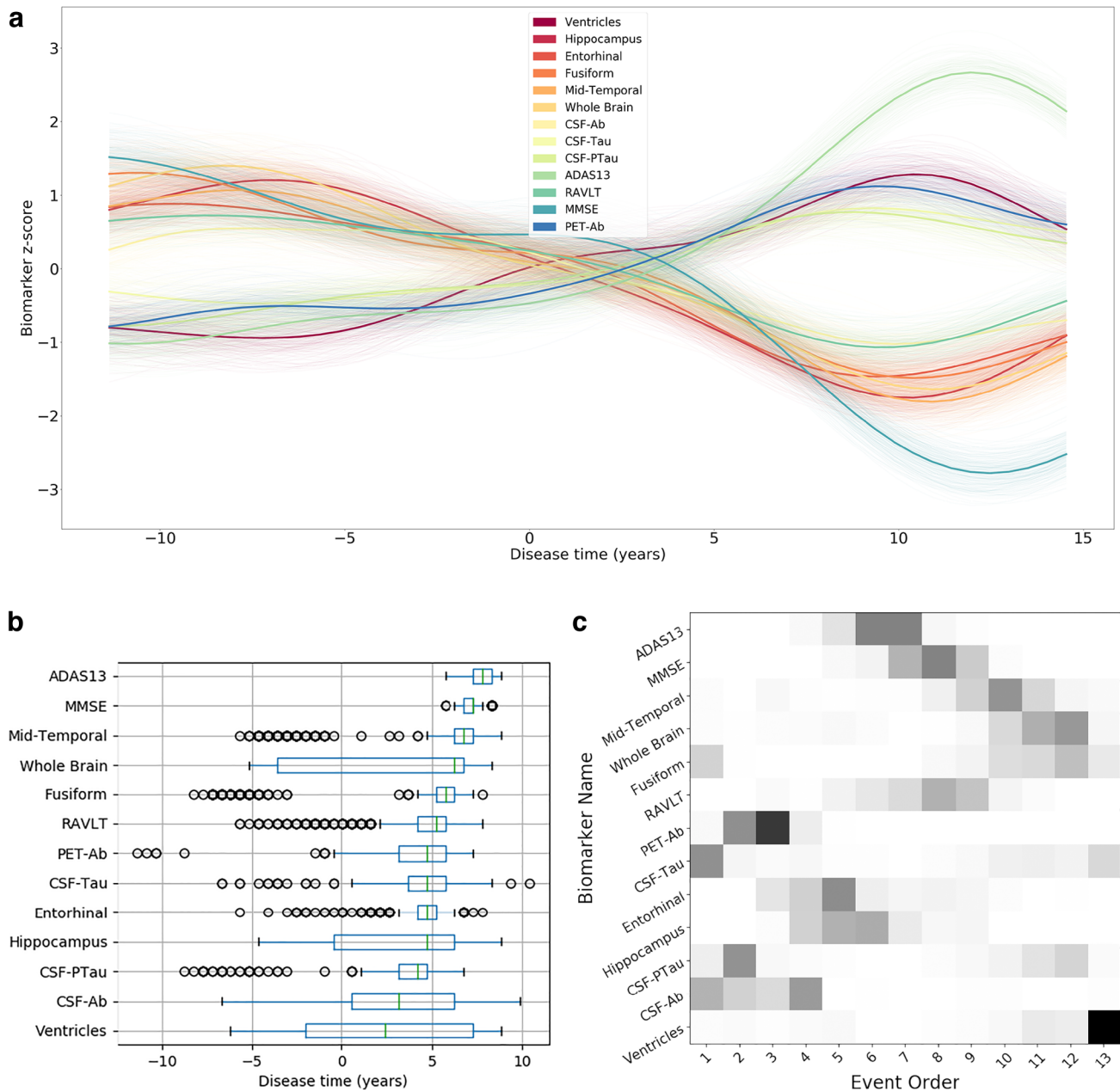


Fig. 3. Biomarker timelines and sequences estimated by two reference disease progression models in AD. (a) Biomarker trajectories obtained by the GPPM from ADNI Dataset 2. Variability in the average trajectories, shown by partially transparent lines, is obtained by taking 200 samples from the model posterior. (b) Timeline of biomarker changes estimated by the GPPM using the point of maximum rate of change across all biomarker trajectories. (c) EBM event sequence obtained from ADNI Dataset 1. Uncertainty in the sequence ordering is represented by shaded boxes, and was estimated using 100 bootstrap samples of the data. To facilitate easy comparison between (b) and (c), the ordering of biomarker labels on the vertical axis in (b) is set identical to the ordering in (c).

that are trained on observed conversion data, that is, we use longitudinal data to estimate conversion rates for individuals classified at baseline into each model stage. To provide an alternative measure of time-to-event, Supplementary Figure S2b shows the time-to-event residual

(difference between observed and predicted) for the three models, calculated by defining the event as the model stage or time-shift that corresponds to all cognitive markers being abnormal. We find that the TEBM provides both the most accurate prediction (TEBM mean

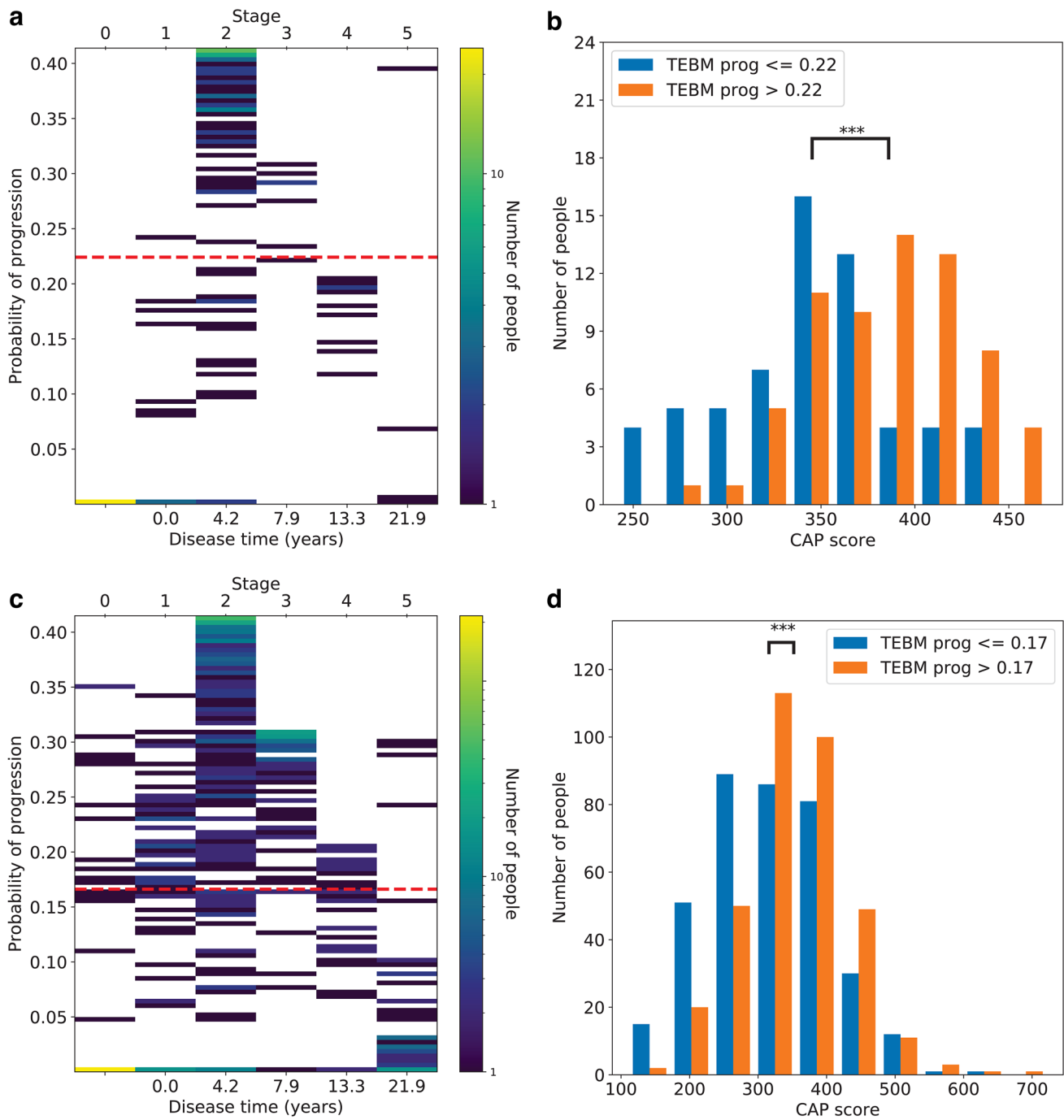


Fig. 4. Within- and out-of-sample model validation in HD. (a) 2D heatmap of the number of individuals distributed according to their disease time (or stage) and progression risk, as estimated by the TEBM using only baseline data from the PreHD group in TRACK-HD. The cut point on progression risk used in (b) is shown by a red dashed line. (b) Genetic burden, as measured by CAP score, for the fast and slow progressing groups. (c) and (d) are the same as (a) and (b) but using the PreHD group from PREDICT-HD with the model trained on TRACK-HD data. The three stars (***) indicate significant difference of the means at $p < 0.001$, under a two-tailed paired t-test. HD, Huntington's disease; TEBM, Temporal Event-Based Model; PreHD, pre-manifest Huntington's disease; CAP, cytosine-adenine-guanine age product.

residual = -0.6 years; EBM mean residual = 4.8 years; GPPM mean residual = -3 years) and the highest precision (TEBM RMSE = 3.1 years; EBM RMSE = 6.6 years; GPPM RMSE = 3.8 years).

2.3. TEBM dichotomises by genetic burden in HD using only baseline data

Figure 4a and c show 2D heatmaps of the number of individuals distributed according to the two predictive variables provided by the TEBM; the disease time (or equivalently, stage), and the progression risk, as estimated by the TEBM trained on TRACK-HD data and tested using only baseline data from PreHD individuals in (a) TRACK-HD (i.e., within-sample), and (c) PREDICT-HD (i.e., out-of-sample).

We observe substantial variability in the progression risk even within a single stage; this information would not be available to staging-only models like the EBM. We use genetic burden, as measured by the cytosine-adenine-guanine (CAG) age product (CAP) score, to validate the predicted progression risk at the group level, under the hypothesis that the fast progressing group will have a higher genetic burden. We use the TEBM to dichotomise the samples into fast and slow progressing groups using a data-driven threshold equal to the mean progression risk across the samples in each dataset (Fig. 4b, d). We find significant differences in mean genetic burden between the groups under a two-tailed paired t-test ($p < 0.001$ in both datasets), with the fast progressing groups having higher genetic burden, as expected. These results provide within- and out-of-sample model validation of the TEBM's ability to predict progression using only baseline data.

2.4. TEBM stratifies by clinical progression rate in AD using only baseline data

Figure 5a shows a 2D heatmap of the number of MCI individuals distributed according to their disease time (or

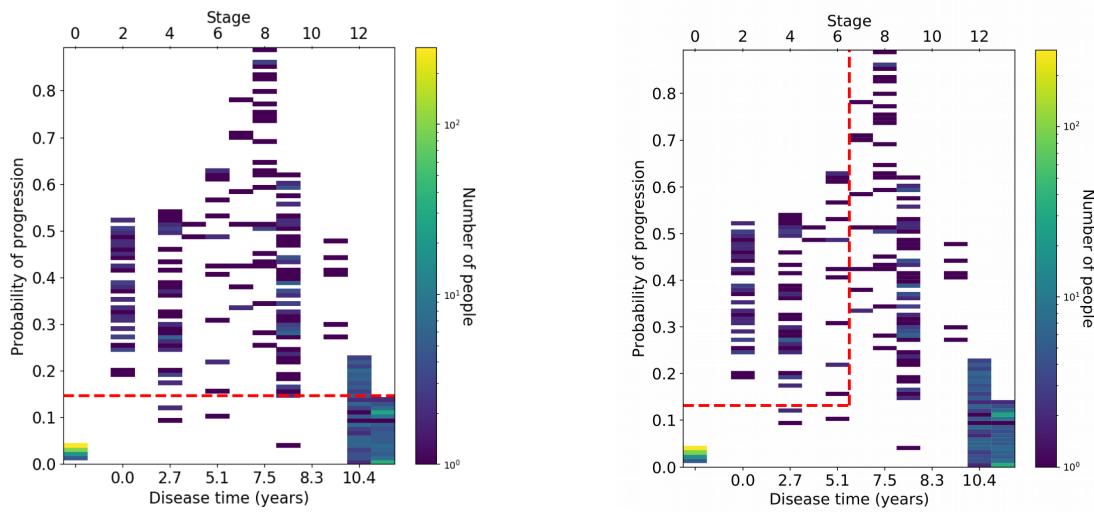
stage) and progression risk, estimated by the TEBM using only baseline data from the ADNI test set. As in Section 2.3, we again observe substantial variability in the progression risk even within a single stage.

We then compare clinical progression, measured by the hold-out variable Clinical Dementia Rating scale Sum of Boxes (CDRSB), between either Figure 5b the fast progressing group ($N = 145$; "TEBM: prog") and the same number of individuals randomly selected from the whole sample ("Random"); or Figure 5c the fast progressing and early-stage group ($N = 64$; "TEBM: stage + prog") and the same number of individuals randomly selected from the early-stage group ("TEBM: stage"). The thresholds used to define the "fast" and "fast and early stage" groups are shown in Figure 5a by dashed red lines, where "early stage" means having a TEBM stage < 7 , that is, before the first cognitive event (ADAS13; see Fig. 2). We again dichotomise into fast and slow progressing groups using a data-driven threshold equal to the mean progression risk across the samples in each dataset. The thresholds on progression risk for the "fast" and "fast and early" groups are slightly different; this is because we calculate the threshold for the latter group after applying the stage cut. We use CDRSB as the outcome variable because it was used as the primary outcome variable in a recent clinical trial in AD (<https://clinicaltrials.gov/ct2/show/results/NCT02477800>), and hypothesise that the fast progressing group will have a higher rate of change. It is clear from Figure 5b and c that that is the case. To confirm, using linear fixed effects models with CDRSB as the dependent variable and observation time, group, and the interaction between observation time and group as independent variables, we find that the dichotomised groups start with approximately equal mean CDRSB and proceed to show a significant difference in the rate of change ($\beta = 1.6$, $p = 4 \times 10^{-16}$ in (b); and $\beta = 1.6$, $p < 2 \times 10^{-16}$ in (c), for the interaction terms, respectively, where β is the regression coefficient term and p is the p-value).

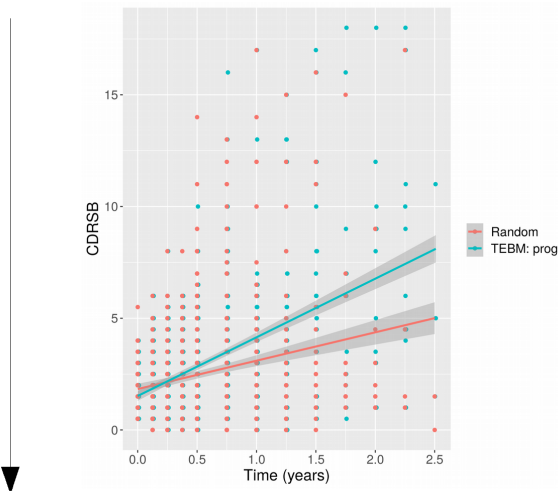
To demonstrate that the TEBM uniquely dichotomises fast and slow progressing groups, we repeat the analysis

Fig. 5. Stratifying by clinical progression and enriching clinical trials using the TEBM. (a) 2D heatmaps of the number of individuals distributed according to their disease time (or stage) and progression risk, as estimated by the TEBM using only baseline data from MCI individuals from the ADNI test set. The cut points on progression risk and stage used to select individuals for (b) and (c), respectively, are shown by dashed red lines. (b) CDRSB as a function of observation time, between the fast progressing group ($N = 145$; "TEBM: prog") and the same number of individuals randomly selected from the whole sample ("Random"). (c) CDRSB as a function of observation time, between the fast progressing and early-stage group ($N = 64$; "TEBM: stage + prog") and the same number of individuals randomly selected from the early-stage group ("TEBM: stage"). (d) Simulation results showing the power of detecting a treatment effect in a general trial for different numbers of participants and treatment effect magnitudes, using CDRSB as the outcome variable, for the "TEBM: prog" and "Random" groups from (b). (e) Equivalent to (d) but for a preventative trial, using the "TEBM: stage + prog" and "TEBM: stage" groups from (c).

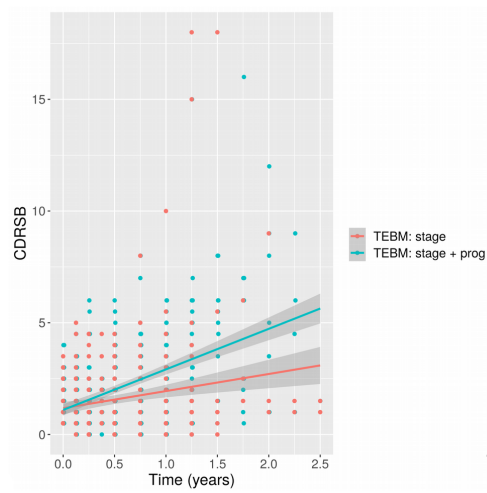
a TEBM progression-stage predictions



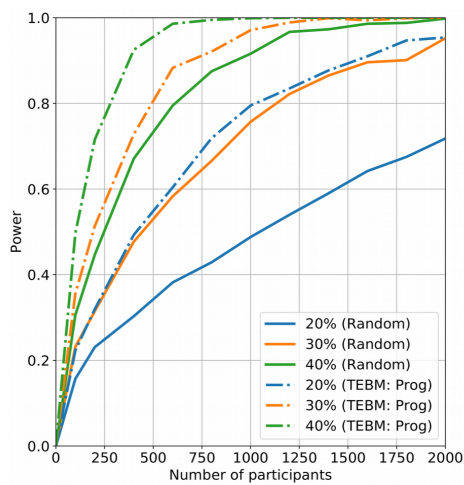
b Select “fast”



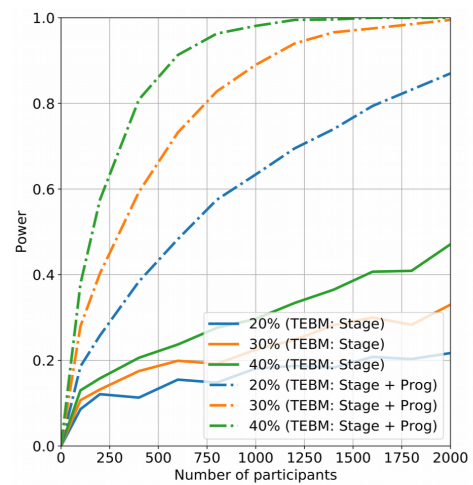
c Select “early stage” and “fast”



d Enrich general clinical trial



e Enrich preventative clinical trial



shown in [Figure 5a, and b](#) using the EBM with post-hoc survival models to estimate a progression risk (see the Methods [section 4.13](#)). We find that the EBM does not provide significant differences between the rates of CDRSB progression and hence cannot dichotomise fast from slow progressing groups (Supplementary Fig. S3a, b).

2.5. TEBM enriches simulated clinical trials

We use the dichotomised groups from [Figure 5b](#) to show that the TEBM can be used to provide substantial improvement in power in a simulated general clinical trial over standard random selection (see the Methods section for more details). [Figure 5d](#) shows graphs of the power to detect a treatment effect of either 20%, 30%, or 40% in CDRSB for varying numbers of people in the trial, for three observations over a 2-year period (baseline plus 2 yearly follow-ups). We find that for both time periods the TEBM-enriched cohort provides at least double the power of the random cohort for the same number of people, and for a 30% treatment effect over 1 year allows the trial to reach power > 0.8 with approximately 750 people, while the equivalent random cohort requires approximately 1750 people.

Finally, we leverage the full predictive capabilities of the TEBM and use the dichotomised groups from [Figure 5c](#) to select a cohort for a preventative clinical trial, that is, before cognitive decline. [Figure 5e](#) shows graphs of the power to detect a treatment effect of 20%, 30%, or 40% in CDRSB for varying numbers of people in the trial, for three observations over a 2-year period (baseline plus 2 yearly follow-ups). We find that the combined criteria are necessary to power preventative clinical trials, whereas the staging-only approach—used by other disease progression models—is substantially under-powered. We also repeat the same simulations but with two observations per individual and find similar results (Supplementary Fig. S4).

3. DISCUSSION

Here, we have introduced the TEBM, a new probabilistic model that learns transition times between successive biomarker events in progressive diseases. This solves a key limitation of event-based disease progression models and provides new capability to identify windows of opportunity to recruit individuals for clinical trials at critical transition points in their disease timeline. We used the TEBM to obtain new timelines of biomarker changes in AD and HD. To validate the TEBM results, we used entirely independent datasets in both AD and HD, and

predicted clinical progression in unseen visits of AD patients better than comparable state-of-the-art disease progression models. We used HD as another exemplar to show the utility of our model, and in particular its ability to extract useful information from small datasets (of order 100 individuals).

A key strength of the TEBM is that it can make probabilistic estimates of progression at the group and individual levels from sparse and irregularly sampled datasets, which are commonplace in real-world medical applications. As such, the TEBM has broad potential application, e.g., in clinical decision support, by informing prognosis; and clinical trial design, by informing biomarker and cohort selection criteria. An additional benefit over deep learning methods is the TEBM's interpretability (we can make clear associations between the input data and the output model predictions), which provides a comprehensible framework for the translation of model predictions to a clinical setting.

We used the TEBM to extract a new timeline of mixed biomarker events in AD ([Fig. 2a](#)). The ordering and timing of key events agrees with clinical observations where available, e.g., abnormality in tau and $A\beta$ ([Bateman et al., 2012](#); [Villemagne et al., 2011, 2013](#)), hippocampus ([Frisoni et al., 2010](#); [Villemagne et al., 2013](#)), and cognitive impairment ([Villemagne et al., 2013](#)). We also directly compared the TEBM AD timeline with the sequence obtained from the EBM and the timeline obtained from the GPPM ([Fig. S3](#)). The comparison highlights the additional information on absolute timescale that the TEBM provides over the EBM. Furthermore, the TEBM naturally provides the ideal structure for estimating event sequences, whereas continuous models such as the GPPM are primarily designed to infer biomarker trajectories ([Bilgel & Jedynak, 2019](#); [Koval et al., 2021](#); [Lorenzi et al., 2019](#); [Oxtoby et al., 2018](#); [Ridha et al., 2006](#); [Staffaroni et al., 2022](#)). In contrast, the TEBM provides the first fine-grained information on the mean and range of time taken to progress between consecutive, clinically interpretable stages. In particular, timescales for pre-clinical AD are of the order of decades ([Masters et al., 2015](#)) but are not well defined, partly due to the difficulty in establishing a suitable reference frame. The TEBM naturally provides such a reference frame; e.g., it can define the pre-clinical phase of AD between tau abnormality and first cognitive impairment (defined by ADAS-13 abnormality in our model) to be 7.5 years (95% CIs: 4.1–12.3 years). Similarly, it can provide new insight into the time between other key outcome measures for clinical trials; e.g., the time between $A\beta$ abnormality and tau abnormality at 2.7 years (95% CIs: 0.5–5.9 years).

These inferences provide new insight into the timescale of pre-clinical AD that can be used to identify time windows for testing new treatments.

Using ADNI data, we also demonstrated that the TEBM can accurately predict the clinical conversion of AD and time-to-event (Supplementary Fig. S2). When trained on time-to-conversion data, we found that the TEBM predicts conversion with an RMSE = 1.8 years, better than either the EBM or GPPM, and comparable or better than values quoted by Bilgel & Jedynak (2019) for their model and other models that arguably use more suitable biomarkers for this task (e.g., CDRSB). However, prediction of conversion is not the primary utility of the TEBM—partly because the model is not directly trained on conversion data—and we provide it here to demonstrate the model's clinical relevance. A more suitable task that utilises the TEBM's event-based structure is prediction of time-to-event, where we found that the TEBM's predictions agreed well with observations (mean residual = -0.6 years). The TEBM's ability to predict time-to-event supports its use for clinical prognosis, where it could inform predictions of the time to an event of interest (e.g., cognitive impairment, or a regional brain abnormality); and in clinical trial design, where it could inform biomarker selection criteria.

Another novel finding is that the TEBM can uniquely dichotomise slow and fast progressing groups over short timescales using only baseline data (Fig. 5b, c). This demonstrates a unique capability of the TEBM among disease progression models to stratify fast from slow progressing groups using only baseline data. Identifying so-called fast progressors is a key challenge in clinical trial design (Dorsey et al., 2015), where the aim is to measure the effect of a treatment with respect to the rate of change of the outcome variable; being able to select fast progressors increases this rate of change, allowing for shorter trials with fewer individuals. We demonstrate this in simulation (Fig. 5d, e), where the fast progressing group identified by the TEBM showed much larger powers compared to random selection, even for clinical trials with only two observations over a single year (Supplementary Fig. S4). However, for the purposes of designing preventative clinical trials, it is necessary to select individuals at the right time before abnormality has accumulated past the point of being treatable. To this aim, we leveraged the full predictive capabilities of the TEBM to simultaneously identify a treatment window before cognitive impairment and a group of fast progressors, facilitating a preventative clinical trial that otherwise would have been substantially under-powered (Fig. 5e). While con-

clusive evidence of the TEBM's ability to enrich clinical trials is only possible using data from real-life clinical trials, our experimental design aims to emulate these conditions as closely as possible, e.g., the multi-site nature of the ADNI dataset reflects a real-life clinical trial. Future work will focus on demonstrating the TEBM subject to the availability of real-life clinical trial data. Furthermore, we will look in more depth at optimising the treatment windows identified by the TEBM (e.g., Fig. 5a), as here we chose fairly simple cuts to demonstrate the method.

In our second application, we used the TEBM to extract a new timeline of biomarker events in HD (Fig. 2b), which we validated with respect to an entirely independent dataset. Furthermore, the ordering and timing of events found by the TEBM is in strong agreement with recently published trajectories of the same markers in HD (Tabrizi et al., 2022); for individuals with 42 CAG repeats, the authors of Tabrizi et al. (2022) estimated the time between putamen and caudate abnormality at approximately 2 years (TEBM: 4.2 years, 95% CIs: 1-10.5 years); TMS abnormality at 6 years (TEBM: 7.9 years, 95% CIs: 3.1-15.3 years); TFC abnormality at 14 years (TEBM: 13.3 years, 95% CIs: 6.3-22.6 years); and SDMT abnormality at 24 years (TEBM: 21.9 years, 95% CIs: 11.4-27.1 years). The TEBM recapitulates these findings within 95% CIs using only a small subset of their dataset, demonstrating its use in small datasets of order 100 individuals. We note that the HD-ISS places SDMT before TFC in its staging system, which is likely driven by differences in the definition of abnormality between the HD-ISS and TEBM. The TEBM also successfully dichotomises groups according to HD genetic burden (defined using individual CAP score), which was not used to train our model (Fig. 4b, d), and which has not been shown previously using only baseline data. Furthermore, we also observed a higher mean progression risk in TRACK-HD than PREDICT-HD, which reflects the known higher mean disease burden in the former dataset (Wijeratne et al., 2020). With respect to model-based analyses, the TEBM finds a similar timescale of regional brain volume changes to other longitudinal disease progression models (Johnson et al., 2020; Wijeratne et al., 2021). In future, we plan to extend the HD analysis by including multiple datasets (e.g., Wijeratne et al. (2020) and Scahill et al. (2020)) to improve coverage of the HD timeline.

Future technical work with the TEBM will focus on developing the model to account for disease heterogeneity, primarily by modelling subtypes of disease progression. The disease heterogeneity in ADNI data has been previously studied by a landmark application of the Sub-

type and Stage Inference (SuStaln) clustering algorithm (Young et al., 2018), which revealed three distinct subtypes of brain atrophy progression. The TEBM has the potential to identify not just distinct trajectories of progression but also sub-groups of progression rate, which could be achieved by integrating the TEBM into the SuStaln algorithm to allow for the inference of both subtype and progression rate (see Young et al., 2023, for a discrete-time formulation). In addition, future work will investigate the broader clinical translation of the TEBM, e.g., using the TEBM trained on ADNI to stage and predict progression in clinical AD datasets. Previous work has demonstrated that EBMs trained on research data can be used to obtain classifications on clinical data (Archetti et al., 2019, 2021). In practice, one would also need to consider potential differences between the training and clinical datasets, e.g., differences between MRI scanners; such differences could be accounted for using harmonisation methods such as Beer et al. (2020). However, even with harmonisation, the datasets used here have substantial ethnic and socio-economic biases (they almost exclusively represent white and middle income people); this limits the potential for widespread translation and highlights the need to design equitable medical studies.

In summary, the TEBM is a new probabilistic model that can extract timelines of biomarker changes in progressive diseases. The TEBM extends the EBM, which found its initial applications in AD and HD but rapidly received more widespread usage and development; the TEBM naturally extends wherever longitudinal data are available, which is becoming more common as communities pull together to collate large patient data sets. As such, the TEBM presents new opportunities for future research and practice by leveraging sparse and irregularly sampled datasets to improve disease understanding and inform preventative clinical trial design, facilitating shorter, smaller trials to accelerate the development of new disease-modifying therapies. More broadly, while here we focused on neurodegenerative diseases, the TEBM could be used to learn timelines in chronic diseases, such as chronic obstructive pulmonary disease, osteoarthritis, and age-related macular degeneration.

4. METHODS

4.1. AD datasets

We use two AD datasets: the TADPOLE challenge dataset (Marinescu et al., 2020), which is a cut of the ADNI dataset, a longitudinal multi-site observational study; and the

OASIS-3 dataset from the OASIS study, a longitudinal single-site observational study (LaMontagne et al., 2019). Basic demographic characteristics of the cohorts used here are summarised in Supplementary Tables S1 and S2.

From ADNI, we select 1737 participants (417 CN: cognitively normal; 872 MCI: mild cognitive impairment; 342 AD: manifest AD; 106 NA: unlabelled), and up to 19 observations per individual (from baseline to 40 months, with a minimum interval of 3 months), corresponding to a total of 12,741 observations. Individuals could have partially missing data; this corresponded to a total fraction of 54% missing data. We use a selection of 13 biofluid, neuroimaging, and clinical test score biomarkers. For the biofluid data, we use three cerebrospinal fluid markers: phosphorylated tau (PTau) and total tau (Tau), and amyloid- β_{1-42} ($A\beta$). For the clinical test score data, we use three cognitive markers: Mini-Mental State Examination (MMSE), Rey Auditory Verbal Learning Test (RAVLT), and the Alzheimer's Disease Assessment Scale (ADAS13). For the neuroimaging data, we select PET- $A\beta$ standardised uptake value ratio (SUVR), and a set of sub-cortical and cortical sMRI regional volumes—the hippocampus, entorhinal, mid-temporal, ventricles, fusiform, and the whole brain—which have been observed to be sensitive to AD pathology (Frisoni et al., 2010).

From OASIS, we select 1332 individuals (949 CN; 22 MCI; 281 AD; 106 NA), and up to 8 observations per individual (from baseline to 13.5 years, with a minimum interval of 6 months), corresponding to a total of 3919 observations. Individuals could have partially missing data; this corresponded to a total fraction of 62% missing data. Because OASIS participants are expected to be at an earlier pre-clinical disease stage than ADNI participants (LaMontagne et al., 2019), we use a subset of the ADNI biomarkers that are expected to occur early in the disease progression. Furthermore, OASIS does not have any biofluid biomarker data, and does not have ADAS13 and RAVLT. Therefore, we use a selection of four neuroimaging and clinical test score biomarkers. For the neuroimaging data, we select PET- $A\beta$ SUVR, and two sMRI regional volumes—the hippocampus and entorhinal. For the clinical test score data, we use MMSE. In both datasets, we segment observation times into the minimum available time between observations, which for ADNI is 3 months, and for OASIS is 6 months.

4.2. ADNI dataset cuts

The GPPM code requires each individual to have at least one measurement of each biomarker across all observa-

tions, otherwise it excludes the individual from the analysis entirely. The TEBM and EBM do not make the same requirement; however, in the AD dataset, using the GPPM selection criteria severely reduces the dataset size (by almost half). Therefore, in the AD analysis, we define two cuts of the AD dataset; the first, which includes all individuals and facilitates unbiased selection of individuals (Dataset 1); and the second, which is a subset of individuals who have at least one biomarker measurement at each observation and facilitates comparison between the TEBM, EBM, and GPPM (Dataset 2). We use Dataset 1 for the analyses in Sections 2.1 & 2.5, and Dataset 2 for the analyses in Section 2.2.

4.3. HD datasets

We use two HD datasets: the TRACK-HD study (Tabrizi et al., 2013), a longitudinal multi-site cohort study; and the PREDICT-HD study (Paulsen et al., 2008), a longitudinal multi-site observational study. Basic demographic characteristics of the cohort are summarised in Supplementary Tables S3 and S4.

From TRACK-HD, we select 356 participants (114 HC: healthy control; 129 PreHD: pre-manifest HD; 113 HD: manifest HD), with up to 4 observations per participant, corresponding to a total of 1204 observations. From PREDICT-HD, we select 948 participants (209 HC: healthy control; 716 PreHD: pre-manifest HD; 21 HD: manifest HD), with up to 7 observations per participant, corresponding to a total of 1712 observations. Individuals could have partially or completely missing data at any time-point; this corresponded to a total fraction of approximately 2% missing data across both datasets. We use a selection of five neuroimaging and clinical test score biomarkers. For the neuroimaging data, we use the volumes of two components of the basal ganglia (caudate, putamen) from sMRI, which are established early markers of HD onset (Tabrizi et al., 2013; Wijeratne et al., 2018). For the clinical test score data, we use Total Motor Score (TMS) as a measure of motor ability, total functional capacity (TFC) as a measure of functional ability, and Symbol Digit Modalities Test (SDMT) as measures of cognitive ability (Tabrizi et al., 2013). As with the AD analysis, we segment observation times into the minimum available time between observations, which is 1 year for both datasets.

4.4. MRI processing

To acquire regional brain volumes from T1-weighted 3T MRI scans, in the AD datasets the TADPOLE challenge

team (Marinescu et al., 2020) segmented scans using FreeSurfer v5.3.0 (Fischl, 2012). In the HD datasets, we segmented scans using the Geodesic Information Flows (GIF) segmentation tool (Cardoso et al., 2015), which is more suitable for deep grey matter structures.

4.5. PET image processing

To acquire an image-based measure of $A\beta$ deposition in the brain in AD, we use AV45 PET scans post-processed to calculate the standard uptake value ratio (SUVR). In the ADNI dataset, we use the variable normalised with respect to the cortical composite region, which is recommended for longitudinal analysis (Landau & Jagust, 2015); in the OASIS dataset, this variable is not available, so we use the variable normalised to the whole cerebellum.

4.6. Data transformation and covariate adjustment

In both the AD and HD analyses, we first normalised the post-processed regional imaging volumes by the individual's total intracranial volume, calculated as the sum of grey matter, white matter, and cerebro-spinal fluid. We also log normalise the biofluid markers in both datasets (ABETA, PTAU, TAU in ADNI; plasma NfL in TRACK-HD). Biomarkers were adjusted for covariates by using linear regression on the cognitively normal (CN) or health control (HC) distributions for AD and HD respectively, with the biomarker as the dependent variable and covariates as the independent variables. The regional volumes were adjusted for baseline age, sex, site, MRI scanner field strength, and total intracranial volume; the clinical test score data were adjusted for baseline age, sex, site, and years of education; and the biofluid measures were adjusted for baseline age, sex, and site.

4.7. Mathematical model

The temporal event-based model (TEBM) is the time generalisation of the event-based model (EBM) (Fonteijn et al., 2011, 2012; Young et al., 2014). Here, we provide only the key equations for the TEBM; see the Supplementary Material for the full model derivation. To formulate the TEBM, we make three main assumptions: *i*) monotonic biomarker dynamics at the group level; *ii*) a consistent event sequence across the whole population; and *iii*) Markov (i.e., “memoryless”) stage transitions at the individual level. The TEBM assumes that each individual $j = 1, \dots, J$ provides measurements of a subset of

biomarkers $i = 1, \dots, I$ at each of $t = 0, \dots, T_j$ time-points. We can write the TEBM total likelihood as:

$$P(Y | \Theta, S) = \prod_{j=1}^J \left[\sum_{k_{j,t=0}}^N P(k_{j,t=0} | S, \pi) \prod_{t=1}^{T_j} P(k_{j,t} | k_{j,t-1}, S, \Delta, Q) \prod_{t=0}^{T_j} \prod_{i=1}^{k_{j,t}} P(Y_{i,j,t} | k_{j,t}, \theta_i^p, S) \prod_{i=k_{j,t}+1}^I P(Y_{i,j,t} | k_{j,t}, \theta_i^c, S) \right]. \quad (1)$$

Here, $S = \{s(1), \dots, s(N)\}$ is a permutation of N events that represents the hidden sequence of events defining the discrete state space for a continuous-time Markov jump process, τ , where an event is the transition of a biomarker from a normal to an abnormal state; $\Theta_j = [\pi, Q, \theta_j]$ are additional model parameters, where π is the initial probability vector with elements π_a , where $a = 1, \dots, N$, that is, π_a is the initial probability of being at stage a ; Q is the transition rate matrix with elements $q_{a,b}$, where $a, b = 1, \dots, N$, that is, $q_{a,b}$ is the transition rate from stage a to b ; Δ is the time period of transitions; $\theta_j = \theta^{p_i} \cup \theta^{c_i}$ are the distribution parameters generating the data for biomarker i (defined in the next paragraph); $k_{j,t} \in 0, \dots, N$ is the latent disease stage for individual j observed at time-point t ; and $Y_{i,j,t}$ is the observed data for biomarker i from individual j at time t . We emphasise that not every individual is required to have more than one time-point; the TEBM can handle individuals with irregularly sampled data, and if a given individual only has a single measurement then their data will inform (1) but not the estimation of $P(k_{j,t} | k_{j,t-1}, \Delta)$.

Following Young et al. (2014), we assume univariate normal distributions for the data, $Y_i \sim \mathcal{N}(\mu_i, \sigma_i)$, and choose a two-component Gaussian mixture model to describe the data likelihood:

$$\prod_{i=1}^I P(Y_{i,j,t} | k_{j,t}, \theta_i, S) = \prod_{i=1}^{k_{j,t}} P(Y_{i,j,t} | k_{j,t}, \theta_i^p, S) \prod_{i=k_{j,t}+1}^I P(Y_{i,j,t} | k_{j,t}, \theta_i^c, S). \quad (2)$$

Here, $\theta_i^p = [\mu_i^p, \sigma_i^p, w_i^p]$ and $\theta_i^c = [\mu_i^c, \sigma_i^c, w_i^c]$ are the mean, μ , standard deviation, σ , and mixture weights, w , for the “abnormal” (i.e., unhealthy) and “normal” (i.e., healthy) distributions, respectively. These distributions are fit prior to inference, which requires our data to contain labels for patients and controls (see Section 4.9); however, once θ_i^p and θ_i^c have been fit, the model can infer S, π, Q without any labels. An advantage of using a

two-component mixture model is that if data $Y_{i,j,t}$ are missing, the two probabilities on the right-hand side of (2) can be set equal and factorised.

4.8. Model inference

We aim to learn the sequence \bar{S} , initial probability vector $\bar{\pi}$, and transition generator matrix \bar{Q} , that maximise the complete log likelihood, $\mathcal{L}(S, \pi, Q) = \log P(Y, k; S, \pi, Q, \theta)$. As described in Section 4.7, we first obtain θ using Gaussian mixture models. We then apply a nested application of the expectation-maximisation (EM) algorithm, which consists of an outer EM algorithm that fits \bar{S} ; and an inner EM algorithm that fits $\bar{\pi}$ and \bar{Q} . For each algorithm, we allow 100 iterations and a tolerance of $1E^{-3}$ of the likelihood between iterations, which we find provides sufficient convergence. Full details of the TEBM inference scheme are provided in the Supplementary Material.

4.9. Model training

To obtain the TEBM data likelihood, we first fit Gaussian mixture models (2) to the biomarker distributions of clinically-labelled “control” and “patient” sub-groups, which we define as the cognitively normal (CN) and Alzheimer’s disease (AD) sub-groups for AD, and the healthy control (HC) and manifest Huntington’s disease (HD) sub-groups for HD. For the application of TEBM to both the AD and HD datasets, we set the diagonal elements of the prior on Q such that the mean sojourn time for each state is 1 year and constrain the transition generator matrix Q to permit forward-only first-order transitions, which reflects the slowly progressive and monotonic nature of AD and HD; and we impose a uniform prior on the initial probability π .

In the AD analysis using OASIS data, we only use the CNs to fit the mixture models and do not use them to fit S, π , and Q , to enable a more direct comparison with the ADNI cohort, which has a ratio of approximately 3:1 cognitively impaired (MCI or AD) to CN, while OASIS has approximately the opposite ratio; furthermore, the OASIS CNs are younger on average than the ADNI CNs by approximately 8 years (see Supplementary Tables S1 and S2). In the HD analysis, we again only use the HCs to fit the mixture models and do not use them to fit S, π , and Q , since HCs are genetically specified and hence should not progress along the event sequence. Furthermore, in the HD analysis using PREDICT-HD data, we use the mixture models fitted to the TRACK-HD data, because there are insufficient manifest HD individuals in the PREDICT-HD dataset. Finally, we use 24 start-points for the outer EM

algorithm for the sequence S , to reduce the chance of fitting to local minima.

For the EBM and GPPM analyses, we use the default parameters as defined by the respective model codes (see Section 4.16) to fit the models, with the exception of the “trade-off” parameter used by the GPPM, which we set equal to 10, as in, e.g., [Wijeratne et al. \(2021\)](#).

4.10. Model stage duration

The expected duration of each stage (sojourn time), δ_a , is given by:

$$\delta_a = \int_0^{\infty} \exp(-\Delta Q_{aa}) d\Delta = -1/q_{aa}. \quad (3)$$

Here, q_{aa} are the diagonal elements of the transition generator matrix Q .

4.11. Model staging and prediction

Given \bar{S} , $\bar{\pi}$, and \bar{Q} , we can use the Viterbi algorithm ([Rabiner, 1989](#)) to estimate an individual’s most likely stage sequence $\bar{k}_j = \{k_{j,0}, k_{j,1}, \dots, k_{j,T_j}\}$ and hence their most likely stage at time t :

$$\bar{k}_{j,t} = \arg \max_k [P(k_{j,t} | \bar{S})]. \quad (4)$$

We can predict the most likely next stage (i.e., future stage) for a given individual over a time period Δ by multiplying the probability distribution at time t by the fitted transition generator matrix evaluated at Δ :

$$\arg \max_k [P(k_{j,t+1} | \bar{S})] = \arg \max_k [P(k_{j,t} | \bar{S}) \cdot \exp(\Delta \bar{Q})]. \quad (5)$$

We also define an individual-level “progression risk,” $r_{j,t}$, that leverages information from both the initial and predicted distributions. First, we calculate the maximum likelihood stage from the initial distribution, $k_{\max} = \arg \max_k [P(k_{j,t} | \bar{S})]$, then we calculate the absolute difference between the probability from this stage in the initial distribution and the probability from the same stage in the predicted distribution:

$$r_{j,t} = |P(k_{j,t} = k_{\max} | \bar{S}) - P(k_{j,t+1} = k_{\max} | \bar{S})|. \quad (6)$$

For a forward-only transition matrix, $r_{j,t}$ will equal zero if the maximum likelihoods from the baseline and predicted likelihood distributions are equal (i.e., zero progression risk), and equal one if they are maximally different. As such, individuals may have non-zero risk of

progression at the final stage if they have greater probability of being at the final stage at the predicted time-point than at baseline. This should reflect an increased probability of abnormality in the corresponding biomarker in the final stage, that is, the risk of progression in abnormality, which is what the measure is capturing.

For the classification task in [Section 2.2](#), the incorporated metric is calculated by multiplying Equations 4 and 6 for $t = 0$. For the progression risk in [Sections 2.3-2.5](#), we choose $\Delta = 2$ years for the time window and set $t = 0$.

4.12. Model uncertainty

In both the AD and HD analyses, we use the training set to fit the TEBM parameters S , Q , and π , and calculate the mean sojourn time for each event according to Equation (3). We estimate the uncertainty in the sojourn time by refitting all model parameters S , Q , and π to 1000 bootstraps of the data, then calculate 95% confidence intervals using the bias-corrected and accelerated (BCa) method. Finally, we calculate the cumulative uncertainty in the sojourn time for event s_n as the cumulative uncertainty propagated quadratically through the event sequence to that event. To calculate the staging uncertainty for a given individual, we take 100 samples from the probability on the right-hand side of Equation 4 to obtain samples of $Y_{j,t}$, then stage using these samples to obtain a distribution of stages. We use these samples to calculate the predicted mean and standard deviation times for each individual.

4.13. Obtaining progression risk from the EBM

To obtain a similar metric of progression as Eqn. 6 from the EBM, we stage individuals using the EBM and then fit Cox proportional hazard models on their EBM stage and observed time, with the event being defined as advancing in stage (as in [Young et al., 2014](#)). We then take one minus the survival probability as the progression risk.

4.14. Predicting age of conversion

Following a similar approach as [Bilgel & Jedynak \(2019\)](#), we predict conversion by first estimating baseline TEBM stage in the training set, then fit a linear regression with observed conversion as the dependent variable and baseline stage as the independent variable; finally, we input the baseline TEBM stages from the test set into the regression model to predict the age of conversion. We use the equivalent approach for the EBM and GPPM, using EBM stage and GPPM time-shift, respectively.

4.15. Clinical trial simulations

We used mixed effects models to obtain power estimates for simulated clinical trials (Jones et al., 2003). Specifically, we first fit a mixed effects model to data from MCI individuals in the test set with the outcome variable of choice as the dependent variable, observation time as the fixed effect, and random effects on the intercept and time. We then use the hyper-parameters of the fitted mixed effects model to simulate the outcome variable with sample size J . The simulated data are then used as the dependent for another mixed effects model, which has observation time, treatment effect, X , and the interaction between time and treatment as fixed effects, and random effects on the intercept and time. We then vary J and X to simulate clinical trials of different sizes and treatment effects. We simulate each trial 1000 times and calculate power for each simulation as equal to one if the magnitude of the time-treatment interaction is more than twice its uncertainty, or zero otherwise; the resulting power is the average over all simulations. We adopt the convention that power $> 80\%$ is considered to have rejected type-II error, with significance assumed under a two-tailed t-test with $\alpha = 0.05$. We use the R statistical software (R Core Team, 2017) with the LMER package.

DATA AND CODE AVAILABILITY

The version of the ADNI dataset that we use is called “Tadpole Challenge Data” and is available to download for users with an ADNI account: <http://adni.loni.usc.edu/data-samples/access-data/>. The version of the OASIS dataset is OASIS-3 and is available to download here: <https://www.oasis-brains.org/>. Requests to access the TRACK-HD and PREDICT-HD (version 4) datasets can be made to the CHDI Foundation: <https://chdifoundation.org/policies/>. Python code for the TEBM and scripts to reproduce the results in this paper are available here: <https://github.com/pawij/tebm>. R code to reproduce the simulations in this paper is available here: <https://github.com/pawij/ctsimulator>. Python code for the EBM is available here: https://github.com/ucl-pond/kde_ebm. Python code for the GPPM is available here: https://gitlab.inria.fr/epione/GP_progression_model_V2.

AUTHOR CONTRIBUTIONS

P.A.W. designed the methodology. P.A.W., A.E., and D.C.A. designed the analysis. J.S.P., R.I.S., C.S., and S.J.T.

contributed to data collection. All authors contributed to interpretation of the data and writing the manuscript.

DECLARATION OF COMPETING INTEREST

The authors declare no competing financial or non-financial interests.

ACKNOWLEDGMENTS

P.A.W. was supported by an MRC Skills Development Fellowship (MR/T027770/1). A.E. was supported by an award from the International Progressive MS Alliance (PA-1412-02420). M.K. was supported by a grant from CHDI Foundation (A-15920). S.J.T. holds a Wellcome Trust Collaborative Award (200181/Z/15/Z) which provides funding for R.I.S. TRACK-HD was funded by CHDI Foundation. N.P.O. is a UKRI Future Leaders Fellow (MR/S03546X/1). PREDICT-HD was primarily funded by NIH grant NS040068. J.S.P. is funded by NIH grants NS082089, NS040068, NS103475, and NS105509. The authors acknowledge funding from the EuroPOND project (Horizon 2020; NPO, LMA, DCA), the E-DADS project (EU JPND; NPO and DCA), the National Institute for Health Research University College London Hospitals Biomedical Research Centre, a Wellcome Trust award (221915/Z/20/Z), and the European Union’s Horizon 2020 research and innovation programme under grant agreement No. 666992. This research was funded in part by the Wellcome Trust (221915/Z/20/Z and 200181/Z/15/Z).

SUPPLEMENTARY MATERIALS

Supplementary material for this article is available with the online version here: https://doi.org/10.1162/imag_a_00010.

REFERENCES

- Archetti, D., Ingala, S., Venkatraghavan, V., Wottschel, V., Young, A. L., Bellio, M., Bron, E. E., Klein, S., Barkhof, F., Alexander, D. C., Oxtoby, N. P., Frisoni, G. B., & Redolfi, A.; for the Alzheimer’s Disease Neuroimaging Initiative, for EuroPOND Consortium. (2019). Multi-study validation of data-driven disease progression models to characterize evolution of biomarkers in Alzheimer’s disease. *Neuroimage Clin*, 24, 101954. <https://doi.org/10.1016/j.nicl.2019.101954>
- Archetti, D., Young, A. L., Oxtoby, N. P., Ferreira, D., Mårtensson, G., Westman, E., Alexander, D. C., Frisoni, G. B., & Alberto, Redolfi; for Alzheimer’s Disease Neuroimaging Initiative and EuroPOND Consortium.

- (2021). Inter-cohort validation of sustain model for Alzheimer's disease. *Front Big Data*, 4, 661110. <https://doi.org/10.3389/fdata.2021.661110>
- Bateman, R. J., Xiong, C., Benzinger, T. L. S., Fagan, A. M., Goate, A., Fox, N. C., Marcus, D. S., Cairns, N. J., Xie, X., Tyler, M. S., Blazey, M., Holtzman, D. M., Santacruz, A., Buckles, V., Oliver, A., Moulder, K., Aisen, P. S., Ghetti, B., Klunk, W. E., ... Morris, J. C. (2012). Clinical and biomarker changes in dominantly inherited Alzheimer's disease. *N Engl J Med*, 367(9), 795–804. <https://doi.org/10.1056/NEJMoa1202753>
- Beer, J. C., Tustison, N. J., Cook, P. A., Davatzikos, C., Sheline, Y. I., Shinohara, R. T., & Linn, K. A.; for the Alzheimer's Disease Neuroimaging Initiative. (2020). Longitudinal combat: A method for harmonizing longitudinal multi-scanner imaging data. *NeuroImage*, 220, 117129. <http://dx.doi.org/10.1016/j.neuroimage.2020.117129>
- Bilgel, M., & Jernigan, B. M. (2019). Predicting time to dementia using a quantitative template of disease progression. *Alzheimers Dement*, 11, 205–215. <https://doi.org/10.1016/j.dadm.2019.01.005>
- Byrne, L. M., Rodrigues, F. B., Blennow, K., Durr, A., Leavitt, B. R., Roos, R. A. C., Scahill, R. I., Tabrizi, S. J., Zetterberg, H., Langbehn, D., & Wild, E. J. (2017). Neurofilament light protein in blood as a potential biomarker of neurodegeneration in Huntington's disease: A retrospective cohort analysis. *Lancet Neurol*, 16, 601–609. [https://doi.org/10.1016/S1474-4422\(17\)30124-2](https://doi.org/10.1016/S1474-4422(17)30124-2)
- Byrne, L. M., Rodrigues, F. B., Johnson, E. B., Wijeratne, P. A., de Vita, E., Alexander, D. C., Palermo, G., Czech, C., Schobel, S., Scahill, R. I., Heslegrave, A., Zetterberg, H., & Wild, E. J. (2018). Evaluation of mutant Huntingtin and neurofilament proteins as potential markers in Huntington's disease. *Sci Transl Med*, 10, eaat7108. <https://doi.org/10.1126/scitranslmed.aat7108>
- Cardoso, M. J., Modat, M., Wolz, R., Melbourne, A., Cash, D., Rueckert, D., & Ourselin, S. (2015). Geodesic information flows: Spatially-variant graphs and their application to segmentation and fusion. *IEEE Trans Med Imaging*, 34(9), 1976–1988. <https://doi.org/10.1109/TMI.2015.2418298>
- Donohue, M. C., Jacqmin-Gadda, H., Le Goff, M., Thomas, R. G., Raman, R., Gamst, A. C., Beckett, L. A., Jack, C. R., Jr., Weiner, M. W., Dartigues, J.-F., & P. S. Aisen. (2014). Estimating long-term multivariate progression from short-term data. *Alzheimers Dement*, 10, S400–S410. <https://doi.org/10.1016/j.jalz.2013.10.003>
- Dorsey, E. R., Venuto, C., Venkataraman, V., Harris, D. A., & Kiebert, K. (2015). Novel methods and technologies for 21st-century clinical trials. *JAMA Neurol*, 72, 582–588. <http://dx.doi.org/10.1001/jama.2014.4524>
- Eshaghi, A., Marinescu, R. V., Young, A. L., Firth, N. C., Prados, F., Cardoso, M. J., Tur, C., De Angelis, F., Cawley, N., Brownlee, W. J., De Stefano, N., Stromillo, M. L., Battaglini, M., Ruggieri, S., Gasperini, C., Filippi, M., Rocca, M. A., Rovira, A., Sastre-Garriga, J., ... Ciccarelli O. (2018). Progression of regional grey matter atrophy in multiple sclerosis. *Brain*, 141(6), 1665–1677. <https://doi.org/10.1093/brain/awy088>
- Eshaghi, A., Young, A. L., Wijeratne, P. A., Prados, F., Arnold, D. L., Narayanan, S., Guttmann, C. R. G., Barkhof, F., Alexander, D. C., Thompson, A. J., Chard, D., & Ciccarelli, O. (2021). Identifying multiple sclerosis subtypes using unsupervised machine learning and MRI data. *Nat Commun*, 12, 2078. <https://doi.org/10.1038/s41467-021-22265-2>
- Firth, N. C., Startin, C. M., Hithersay, R., Hamburg, S., Wijeratne, P. A., Mok, K. Y., Hardy, J., & Alexander, D. C.; The LonDownS Consortium, André Strydom. (2018). Aging related cognitive changes associated with Alzheimer's disease in Down syndrome. *Ann Clin Transl Neurol*, 5, 1665–1677. <https://doi.org/10.1002/acn3.571>
- Fischl, B. (2012). Freesurfer. *NeuroImage*, 62, 774–781. <https://doi.org/10.1016/j.neuroimage.2012.01.021>
- Fonteijn, H. M., Clarkson, M. J., Modat, M., Barnes, J., Lehmann, M., Ourselin, S., Fox N. C., & Alexander, D. C. (2011). An event-based disease progression model and its application to familial Alzheimer's disease. *Inf Process Med Imaging*, 6801, 748–759. https://doi.org/10.1007/978-3-642-22092-0_61
- Fonteijn, H. M., Modat, M., Clarkson, M. J., Barnes, J., Lehmann, M., Hobbs, N. Z., Scahill, R. I., Tabrizi, S. J., Ourselin, S., Fox, N. C., & Alexander, D. C. (2012). An event-based model for disease progression and its application in familial Alzheimer's disease and Huntington's disease. *NeuroImage*, 60, 1880–1889. <https://doi.org/10.1016/j.neuroimage.2012.01.062>
- Frisoni, G. B., Fox, N. C., Jack, C. R., Scheltens, P., & Thompson, P. M. (2010). The clinical use of structural MRI in Alzheimer disease. *Nat Rev Neurol*, 6, 67–77. <http://dx.doi.org/10.1038/nrneuro.2009.215>
- Gabel, M. C., Broad, R. J., Young, A. L., Abrahams, S., Bastin, M. E., Menke, R. A. L., Al-Chalabi, A., Goldstein, L. H., Tsermentseli, S., Alexander, D. C., Turner, M. R., Nigel Leigh, P., & Cercignani, M. (2020). Evolution of white matter damage in amyotrophic lateral sclerosis. *Ann Clin Transl Neurol*, 7, 722–732. <https://doi.org/10.1002/acn3.51035>
- Hadjichrysanthou, C., Evans, S., Bajaj, S., Siakallis, L. C., McRae-McKee, K., de Wolf, F., & Anderson, R. M.; the Alzheimer's Disease Neuroimaging Initiative. (2020). The dynamics of biomarkers across the clinical spectrum of Alzheimer's disease. *Alzheimers Res Ther*, 12. <https://doi.org/10.1186/s13195-020-00636-z>
- Hempel, H., Cummings, J., Blennow, K., Gao, P., Jack, C. R., Jr., & Vergallo, A. (2021). Developing the atx(n) classification for use across the Alzheimer disease continuum. *Nat Rev Neurol*, 17, 580–589. <https://doi.org/10.1038/s41582-021-00520-w>
- Johnson, E. B., Ziegler, G., Penny, W., Rees, G., Tabrizi, S. J., Scahill, R. I., & Gregory S. (2020). Dynamics of cortical degeneration over a decade in Huntington's disease. *Biol Psychiatry*, 89, 807–816. <https://doi.org/10.1016/j.biopsych.2020.11.009>
- Jones, S. R., Carley, S., & Harrison, M. (2003). An introduction to power and sample size estimation. *Emerg Med J*, 20, 453–458. <https://doi.org/10.1136/emj.20.5.453>
- Knopman, D. S., Amieva, H., Petersen, R. C., Chételat, G., Holtzman, D. M., Hyman, B. T., Nixon, R. A., & Jones, D. T. (2021). Alzheimer disease. *Nat Rev Dis Primers*. <https://doi.org/10.1038/s41572-021-00269-y>
- Koval, I., Bône, A., Louis, M., Lartigue, T., Bottani, S., Marcoux, A., Samper-González, J., Burgos, N., Charlier, B., Bertrand, A., Epelbaum, S., Colliot, O., Allasoussi, S., & Durrleman, S. (2021). AD course map charts Alzheimer's disease progression. *Sci Rep*, 11, 8020. <https://doi.org/10.1038/s41598-021-87434-1>

- LaMontagne, P. J., Benzinger, T. L. S., Morris, J. C., Keefe, S., Hornbeck, R., Xiong, C., Grant, E., Hassenstab, J., Moulder, K., Vlassenko, A. G., Raichle, M. E., Cruchaga, C., & Marcus, D. (2019). Oasis-3: Longitudinal neuroimaging, clinical, and cognitive dataset for normal aging and Alzheimer disease. *medRxiv*. <https://doi.org/10.1101/2019.12.13.19014902>
- Landau, S., & Jagust, W. (2015). Florbetapir processing methods. https://adni.bitbucket.io/reference/docs/UCBERKELEYAV45/ADNI_AV45_Methods_JagustLab_06.25.15.pdf
- Li, D., Iddi, S., Aisen, P. S., Thompson, W. K., & Donohue, M. C.; for the Alzheimer's Disease Neuroimaging Initiative. (2019). The relative efficiency of time-to-progression and continuous measures of cognition in presymptomatic Alzheimer's disease. *Alzheimers Dement (N Y)*, 5, 308–318. <https://doi.org/10.1016/j.trci.2019.04.004>
- Liu, Y. Y., Li, S., Li, F., Song, L., & Rehg, J. M. (2015). Efficient learning of continuous-time hidden Markov models for disease progression. *Adv Neural Inf Process Syst*, 28, 3599–3607. <https://www.ncbi.nlm.nih.gov/pmc/articles/PMC4804157/>
- Lorenzi, M., Filippone, M., Frisoni, G. B., Alexander, D. C., & Ourselin, S.; for the Alzheimer's Disease Neuroimaging Initiative. (2019). Probabilistic disease progression modeling to characterize diagnostic uncertainty: Application to staging and prediction in Alzheimer's disease. *NeuroImage*, 190, 56–68. <https://doi.org/10.1016/j.neuroimage.2017.08.059>
- Marinescu, R. V., Oxtoby, N. P., Young, A. L., Bron, E. E., Toga, A. W., Weiner, M. W., Barkhof, F., Fox, N. C., Eshaghi, A., Toni, T., Salaterski, M., Lunina, V., Ansari, M., Durrleman, S., Lu, P., Iddi, S., Li, D., Thompson, W. K., Donohue, M. C., ... Alexander, D. C. (2020). The Alzheimer's disease prediction of longitudinal evolution (tadpole) challenge: Results after 1 year follow-up. *arXiv*. <https://arxiv.org/abs/2002.03419>
- Masters, C. L., Bateman, R., Blennow, K., Rowe, C. C., Sperling, R. A., & Cummings, J. L. (2015). Alzheimer's disease. *Nat Rev Dis Primers*, 1, 15056. <http://dx.doi.org/10.1038/nrdp.2015.56>
- O'Connor, A., Weston, P. S. J., Pavisic, I. M., Ryan, N. S., Collins, J. D., Lu, K., Crutch, S. J., Alexander, D. C., Fox, N. C., & Oxtoby, N. P. (2020). Quantitative detection and staging of presymptomatic cognitive decline in familial Alzheimer's disease: A retrospective cohort analysis. *Alzheimers Res Ther*, 12(1), 126. <https://doi.org/10.1186/s13195-020-00695-2>
- Oxtoby, N. P., & Alexander, D. C. (2017). Imaging plus x: Multimodal models of neurodegenerative disease. *Curr Opin Neurol*, 30(4), 371–379. <http://dx.doi.org/10.1097/WCO.0000000000000460>
- Oxtoby, N. P., Leyland, L. A., Aksman, L. M., Thomas, G. E. C., Bunting, E. L., Wijeratne, P. A., Young, A. L., Zarkali, A., Tan, M. M. X., Bremner, F. D., Keane, P. A., Morris, H. R., Schrag, A. E., Alexander, D. C., & Weil, R. S. (2021). Sequence of clinical and neurodegeneration events in Parkinson's disease progression. *Brain*, 144, 975–988. <https://doi.org/10.1093/brain/awaa461>
- Oxtoby, N. P., Young, A. L., Cash, D. M., Benzinger, T. L. S., Fagan, A. M., Morris, J. C., Bateman, R. J., Fox, N. C., Schott, J. M., & Alexander, D. C. (2018). Data-driven models of dominantly-inherited Alzheimer's disease progression. *Brain*, 141, 1529–1544. <https://doi.org/10.1093/brain/awy050>
- Pascuzzo, R., Oxtoby, N. P., Young, A. L., Blevins, J., Castelli, G., Garbarino, S., Cohen, M. L., Schonberger, L. B., Gambetti, P., Appleby, B. S., Alexander, D. C., & Bizzi, A. (2020). Prion propagation estimated from brain diffusion MRI is subtype dependent in sporadic Creutzfeldt–Jakob disease. *Acta Neuropathol*, 140, 169–181. <https://doi.org/10.1007/s00401-020-02168-0>
- Paulsen, J. S., Langbehn, D. R., Stout, J. C., Aylward, E., Ross, C. A., Nance, M., Guttman, M., Johnson, S., MacDonald, M., Beglinger, L. J., Duff, K., Kayson, E., Biglan, K., Shoulson, I., Oakes, D., & Hayden, M.; Predict-HD Investigators and Coordinators of the Huntington Study Group. (2008). Detection of Huntington's disease decades before diagnosis: The predict-HD study. *J Neurol Neurosurg Psychiatry*, 79, 874–880. <https://dx.doi.org/10.1136/jnnp.2007.128728>
- Prince, M., Bryce, R., Albanese, E., Wimo, A., Ribeiro, W., & Ferri, C. P. (2013). The global prevalence of dementia: A systematic review and metaanalysis. *Alzheimer's Dement*, 9, 63–75. <https://doi.org/10.1016/j.jalz.2012.11.007>
- R Core Team. (2017). R: A language and environment for statistical computing. <https://www.R-project.org/>
- Rabiner, L. (1989). A tutorial on hidden markov models and selected applications in speech recognition. *Proc IEEE*, 77, 257–286. <https://doi.org/10.1109/5.18626>
- Ridha, B. H., Barnes, J., Bartlett, J. W., Godbolt, A., Pepple, T., Rossor, M. N., & Fox, N. C. (2006). Tracking atrophy progression in familial Alzheimer's disease: A serial MRI study. *Lancet Neurol*, 5, 828–834. [https://doi.org/10.1016/S1474-4422\(06\)70550-6](https://doi.org/10.1016/S1474-4422(06)70550-6)
- Scahill, R. I., Zeun, P., Osborne-Crowley, K., Johnson, E. B., Gregory, S., Parker, C., Lowe, J., Nair, A., O'Callaghan, C., Langley, C., Papoutsis, M., McColgan, P., Estevez-Fraga, C., Fayer, K., Wellington, H., Rodrigues, F. B., Byrne, L. M., Heselgrave, A., Hyare, H., ... Tabrizi, S. J. (2020). Biological and clinical characteristics of gene carriers far from predicted onset in the Huntington's disease young adult study (HD-YAS): A cross-sectional analysis. *Lancet Neurol*, 19, 502–512. [https://doi.org/10.1016/S1474-4422\(20\)30143-5](https://doi.org/10.1016/S1474-4422(20)30143-5)
- Schiratti, J. B., Allasonnière, S., Colliot, O., & Durrleman, S. (2017). A Bayesian mixed-effects model to learn trajectories of changes from repeated manifold-valued observations. *J Mach Learn Res*, 18, 1–33. <https://jmlr.csail.mit.edu/papers/volume18/17-197/17-197.pdf>
- Staffaroni, A. M., Quintana, M., Wendelberger, B., Heuer, H. W., Russell, L. L., Cobigo, Y., Wolf, A., Matt Goh, S.-Y., Petrucelli, L., Gendron, T. F., Heller, C., Clark, A. L., Taylor, J. C., Wise, A., Ong, E., Forsberg, L., Brushaber, D., Rojas, J. C., VandeVrede, L., ... Frontotemporal Dementia Prevention Initiative (FPI) Investigators. (2022). Temporal order of clinical and biomarker changes in familial frontotemporal dementia. *Nat Med*, 28, 2194–2206. <https://doi.org/10.1038/s41591-022-01942-9>
- Sun, Z., Ghosh, S., Li, Y., Cheng, Y., Mohan, A., Sampaio, C., & Hu, J. (2019). A probabilistic disease progression modeling approach and its application to integrated Huntington's disease observational data. *JAMIA Open*, 2, 123–130. <https://doi.org/10.1093/jamiaopen/ooy060>
- Tabrizi, S. J., Scahill, R. I., Owen, G., Durr, A., Leavitt, B. R., Roos, R. A., Borowsky, B., Landwehrmeyer, B., Frost, C., Johnson, H., Craufurd, D., Reilmann, R., Stout, J. C., & Langbehn, D. R.; TRACK-HD Investigators. (2013). Predictors of phenotypic progression and disease

- onset in premanifest and early-stage Huntington's disease in the TRACK-HD study: Analysis of 36-month observational data. *Lancet Neurol*, 12, 637–649. [https://doi.org/10.1016/S1474-4422\(13\)70088-7](https://doi.org/10.1016/S1474-4422(13)70088-7)
- Tabrizi, S. J., Schobel, S., Gantman, E. C., Mansbach, A., Borowsky, B., Konstantinova, P., Mestre, T. A., Panagoulas, J., Ross, C. A., Zauderer, M., Mullin, A. P., Romero, K., Sivakumaran, S., Turner, E. C., Long, J. D., & Sampaio, C.; Huntington's Disease Regulatory Science Consortium (HD-RSC). (2022). A biological classification of Huntington's disease: The integrated staging system. *Lancet Neurol*, 21(7):632–644. [https://doi.org/10.1016/S1474-4422\(22\)00120-X](https://doi.org/10.1016/S1474-4422(22)00120-X)
- Venkatraghavan, V., Bron, E. E., Niessen, W. J., & Klein, S.; Alzheimer's Disease Neuroimaging Initiative. (2019). Disease progression timeline estimation for Alzheimer's disease using discriminative event based modeling. *NeuroImage*, 186, 518–532. <https://doi.org/10.1016/j.neuroimage.2018.11.024>
- Villemagne, V. L., Burnham, S., Bourgeat, P., Brown, B., Ellis, K. A., Salvado, O., Szoëke, C., Lance Macaulay, S., Martins, R., Maruff, P., Ames, D., Rowe, C. C., & Masters, C. L.; Australian Imaging Biomarkers and Lifestyle (AIBL) Research Group. (2013). Amyloid β deposition, neurodegeneration, and cognitive decline in sporadic Alzheimer's disease: A prospective cohort study. *Lancet Neurol*, 12, 357–367. [https://doi.org/10.1016/S1474-4422\(13\)70044-9](https://doi.org/10.1016/S1474-4422(13)70044-9)
- Villemagne, V. L., Pike, K. E., Chételat, G., Ellis, K. A., Mulligan, R. S., Bourgeat, P., Ackermann, U., Jones, G., Szoëke, C., Salvado, O., Martins, R., O'Keefe, G., Mathis, C. A., Klunk, W. E., Ames, D., Masters, C. L., & Rowe, C. C. (2011). Longitudinal assessment of a β and cognition in aging and Alzheimer disease. *Ann Neurol*, 69, 181–192. <https://doi.org/10.1002/ana.22248>
- Vogel, J. W., Young, A. L., Oxtoby, N. P., Smith, R., Ossenkoppele, R., Strandberg, O. T., La Joie, R., Aksman, L. M., Grothe, M. J., Iturria-Medina, Y.; Alzheimer's Disease Neuroimaging Initiative; Pontecorvo, M. J., Devous, M. D., Rabinovici, G. D., Alexander, D. C., Lyoo, C. H., Evans, A. C., & Hansson, O. (2021). Four distinct trajectories of tau deposition identified in Alzheimer's disease. *Nat Med*, 27, 871–881. <https://doi.org/10.1038/s41591-021-01309-6>
- Wijeratne, P. A., Garbarino, S., Gregory, S., Johnson, E. B., Scahill, R. I., Paulsen, J. S., Tabrizi, S. J., Lorenzi, M., & Alexander, D. C. (2021). Revealing the timeline of structural MRI changes in premanifest to manifest Huntington disease. *Neuro Genet*, 7, e617. <https://doi.org/10.1212/NXG.0000000000000617>
- Wijeratne, P. A., Johnson, E. B., Eshaghi, A., Aksman, L., Gregory, S., Johnson, H. J., Poudel, G. R., Mohan, A., Sampaio, C., Georgiou-Karistianis, N., Paulsen, J. S., Tabrizi, S. J., Scahill, R. I.; IMAGE-HD, PREDICT-HD, and TRACK-HD Investigators; & Alexander, D. C. (2020). Robust markers and sample sizes for multicenter trials of Huntington disease. *Ann Neurol*, 87, 751–762. <https://doi.org/10.1002/ana.25709>
- Wijeratne, P. A., Young, A. L., Oxtoby, N. P., Marinescu, R. V., Firth, N. C., Johnson, E. B., Mohan, A., Sampaio, C., Scahill, R. I., Tabrizi, S. J., & Alexander, D. C. (2018). An image-based model of brain volume biomarker changes in Huntington's disease. *Ann Clin Transl Neurol*, 5, 570–582. <https://doi.org/10.1002/acn3.558>
- Williams, J. P., Storlie, C. B., Therneau, T. M., Jack, C. R., Jr., & Hannig, J. (2020). A Bayesian approach to multistate hidden Markov models: Application to dementia progression. *J Am Stat Assoc*, 115, 16–31. <https://doi.org/10.1080/01621459.2019.1594831>
- Young, A. L., Aksman, L., Alexander, D. C., & Wijeratne, P. A.; for the Alzheimer's Disease Neuroimaging Initiative. (2023). Subtype and stage inference with timescales. *Lect Notes Comput Sci*, 13939, 15–26. https://doi.org/10.1007/978-3-031-34048-2_2
- Young, A. L., Marinescu, R. V., Oxtoby, N. P., Bocchetta, M., Yong, K., Firth, N. C., Cash, D. M., Thomas, D. L., Dick, K. M., Cardoso, J., van Swieten, J., Borroni, B., Galimberti, D., Masellis, M., Tartaglia, M. C., Rowe, J. B., Graff, C., Tagliavini, F., Frisoni, G. B., ... The Genetic FTD Initiative (GENFI) & The Alzheimer's Disease Neuroimaging Initiative (ADNI). (2018). Uncovering the heterogeneity and temporal complexity of neurodegenerative diseases with subtype and stage inference. *Nat Commun*, 9. <https://doi.org/10.1038/s41467-018-05892-0>
- Young, A. L., Oxtoby, N. P., Daga, P., Cash, D. M., Fox, N. C., Ourselin, S., Schott, J. M., & Alexander, D. C.; Alzheimer's Disease Neuroimaging Initiative. (2014). A data-driven model of biomarker changes in sporadic Alzheimer's disease. *Brain*, 137, 2564–2577. <https://doi.org/10.1093/brain/awu176>